Journal of
Plankton Research

academic.oup.com/plankt

J. Plankton Res. (2021) 1–15. doi:10.1093/plankt/fbab008

BLOOFINZ - Gulf of Mexico

Mesozooplankton biomass, grazing and trophic structure in the bluefin tuna spawning area of the oceanic Gulf of Mexico

MICHAEL R. LANDRY* AND RASMUS SWALETHORP

SCRIPPS INSTITUTION OF OCEANOGRAPHY, UNIVERSITY OF CALIFORNIA, SAN DIEGO, 9500 GILMAN DR., LA JOLLA, CA 92093-0227, USA

*CORRESPONDING AUTHOR: mlandry@ucsd.edu

Received October 13, 2020; editorial decision January 13, 2021; accepted February 1, 2021

Corresponding editor: Xabier Irigoyen

We investigated size-fractioned biomass, isotopes and grazing of mesozooplankton communities in the larval habitat of Atlantic bluefin tuna (ABT) in the oceanic Gulf of Mexico (GoM) during the peak spawning month of May. Euphotic-zone biomass ranged from 101 to 513 mg C m^{-2} during the day and 216 to 798 mg C m^{-2} at night. Grazing varied from 0.1 to 1.0 mg Chl*a* m^{-2} d^{-1}, averaging 1–3% of phytoplankton Chl*a* consumed d^{-1}. Carnivorous taxa dominated the biomass of > 1-mm zooplankton (78% day; 60% night), while only 13% of smaller zooplankton were carnivores. δ^{15}N enrichment between small and large sizes indicates a 0.5–0.6 trophic-step difference. Although characteristics of GoM zooplankton are generally similar to those of remote oligotrophic subtropical regions, zooplankton stocks in the ABT larval habitat are disproportionately high relative to primary production, compared with HOT and BATS averages. Growth-grazing balances for phytoplankton were resolved with a statistically insignificant residual, and trophic fluxes from local productivity were sufficient to satisfy C demand of suspension feeding mesozooplankton. While carnivore C demand was met by local processes in the central GoM, experiments closer to the coastal margin suggest the need for a lateral subsidy of zooplankton biomass to the oceanic region.

KEYWORDS: zooplankton; biomass; subtropical; oligotrophic; growth-grazing balance; production; carbon demand; suspension feeders; carnivores; migrants; active export

available online at academic.oup.com/plankt

INTRODUCTION

The central role of mesozooplankton as trophic intermediaries between primary producers and fish is well recognized in the classic paradigm of marine food webs (Hardy, 1924) and in studies of larval fish ecology, where the temporal matching of prey resources to the needs of larvae in seasonally dynamic environments is often viewed as a critical determinant of recruitment success (Hjort, 1914; Cushing, 1990). In less dynamic larval nursery areas, such as oligotrophic subtropical waters, relationships between fish larvae and zooplankton prey are likely just as important, though more subtle and nuanced (Llopiz *et al*., 2014; Landry *et al*., 2019). For example, like many tuna and billfish species, Atlantic bluefin tuna (ABT, *Thunnus thynnus*) spawn in nutritionally dilute subtropical waters rather than in more-productive adjacent coastal margins as an apparent tradeoff between larval starvation and predation risks (Bakun and Broad, 2003; Bakun, 2013; Shropshire *et al*., this issue). Further complicating interpretation of this strategy, however, ABT larvae are concentrated in fronts and eddies rather than randomly distributed (Bakun, 2006, 2013; Alemany *et al*., 2010; Lindo-Atichati *et al*., 2012), suggesting that specific properties of mesoscale habitats might matter more to larval success than temporal dynamics or mean open-ocean conditions.

Extensive sampling of ABT larvae in the Gulf of Mexico (GoM) since the 1970s has defined narrow environmental windows in which ABT can be found in oceanic waters of the GoM, as well as their particular prevalence in the outer rings of anticyclonic loop eddies that spin off periodically from the Loop Current (Muhling *et al*., 2010, 2011; Lindo-Atichati *et al*., 2012). Domingues *et al*. (2016) linked these relationships to satellite measurements of seasurface height and temperature, establishing a dimensionless index that both successfully captured the general features of larval spatial distributions and temporal variability in the GoM and also explained 58% of interannual stock recruitment variability over a two-decade period (1993–2011). The trophic ecology of ABT larval habit, however, is entirely unexplored. Coherent plankton foodweb studies have not been done in any oceanic waters of the GoM, and there are no prior estimates of mesozooplankton carbon biomass or community grazing in the region. The present study thus addresses a void in basic knowledge of regional ecology while also contributing to a broader system-level process investigation of ABT larval habitat in the oceanic GoM (Gerard *et al*., this issue).

As part of the BLOOFINZ-GoM project (Bluefin Larvae in Oligotrophic Ocean Foodwebs, Investigation of Nitrogen to Zooplankton in the GoM), we investigated biomass and grazing rates of mesozooplankton communities in ABT larval habitat in 2017 and 2018 during the peak spawning month of May. The use of similar methodology allows us compare zooplankton and environmental characteristics in the GoM to those at oligotrophic subtropical sites in the Atlantic and Pacific Oceans that have been systematically studied for decades, and to process studies in other warm-water open-ocean systems. We further draw upon results from companion studies of phytoplankton production (Yingling *et al*., this issue) and phytoplankton growth and microzooplankton grazing (Landry *et al*., this issue) to put zooplankton biomass and grazing in the context of broader trophic fluxes. From these, we address the questions: How much does mesozooplankton grazing contribute to the balance of phytoplankton growth rate and fates in GoM larval ABT habitat? Are trophic fluxes in these waters sufficient to satisfy the carbon demands of actively growing zooplankton? What are the relative magnitudes of trophic flows to mesozooplankton in these areas?

METHODS

Zooplankton sample collection

Mesozooplankton samples were taken in offshore oligotrophic waters of the GoM during BLOOFINZ-GoM cruises NF1704 (7 May–2 June 2017) and NF1802 (27 April–20 May 2018) on NOAA Ship *Nancy Foster*. Sampling was guided by the habitat index model of Domingues *et al.* (2016) based on real-time satellite imagery (Gerard *et al*., this issue). Over the two cruises, five quasi-Lagrangian process studies, hereafter "cycles" C1–C5, of 2–4-day duration were conducted following the paths of a satellite-tracked drifter with a mixed-layer drogue (Fig. 1; Landry *et al*., 2009). Substantial abundances of ABT larvae were found in mixed-layer (upper 25 m) waters during C1 (2017) and C5 (2018) (Shiroza *et al*., this issue). During cycle experiments, we sampled each mid-day (1100–1300) and mid-night (23:00–01:00) with a 1-m diameter ring net (0.2-mm Nitex mesh) towed obliquely through the euphotic zone at a ship speed of ∼1.5 kt. Additional transect samples (T1 and T2) were taken across frontal features at the beginning of the 2018 cruise at irregular times of day (mostly afternoons to evenings between 13:30 and 20:20). Tow depth was controlled directly by shipboard readout from a pressure sensor at the point of net attachment on the hydrowire. Tow distance and volume filtered were measured with a calibrated General Oceanics flowmeter (GO, Miami, FL) attached across the net mouth, assuming 100% filtration efficiency. For NF1704, pressure rating of the hydrowire depth sensor limited net tows to 100-m depth. For NF1802, mean tow depth was 133 ± 2 m.

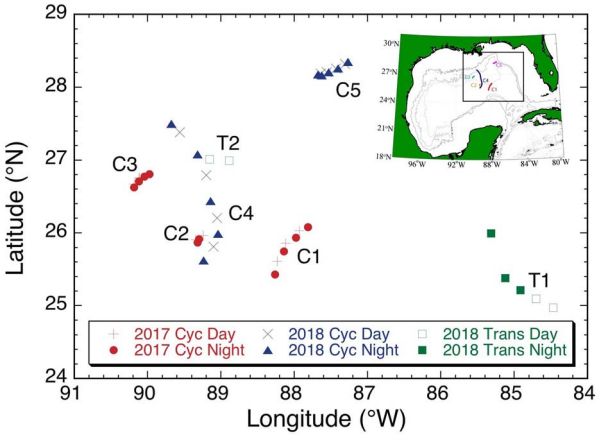

Fig. 1. Sampling locations for mesozooplankton day and night net tows in the GoM. Traces in map inlay depict drift trajectories of Cycles 1–3 in May 2017 and C4–5 in May 2018. Additional transect sampling (T1 and T2) was done in 2018.

Upon retrieval, cod-end contents were anesthetized with CO_2 (ice-cold soda water; Kleppel and Pieper 1984) to slow metabolism and gut evacuation and immediately split with a Folsom plankton splitter. Half of the tow was preserved in borate-buffered 5% formalin. The remaining half was size fractioned by wet sieving through nested screens of 5, 2, 1, 0.5 and 0.2-mm Nitex mesh to produce 5 size classes of 0.2–0.5, 0.5–1, 1–2, 2–5 and 5+ mm. Organisms retained on each mesh were concentrated onto separate pre-weighed filters (47-mm diameter) of 0.2-mm Nitex, rinsed with isotonic ammonium formate solution to remove interstitial sea salt, then placed in individual petri dishes and frozen at −80°C for later analysis. On several occasions, we collected small pyrosomes (5–8 cm) that were too few to subsample quantitatively. We removed these prior to splitting and size fractioning and froze them separately in 50-mL Falcon tubes for weighing and gut pigment analyses.

Biomass and stable isotope analyses

In the laboratory, frozen size-fractioned zooplankton on Nitex filters were thawed, set briefly on blotting paper to remove excess water and weighed moist for total sample wet weight (WW). Wet samples were subsampled for gut pigments by removing replicate portions of the biomass and recording weights before and after each subsampling (fraction of total WW removed). The remaining wet biomass on the filters was oven dried at 60°C for 24 h before weighing dry for the dry weight to wet weight ratio (DW:WW). For each size fraction, zooplankton DW (mg m^{-2}) was calculated from the measured WW (less initial filter weight), DW:WW ratio, measured volume and depth of tow, and fraction of sample analyzed. The remaining dried sample was subsequently scraped off the filter, ground to a powder and subsampled by weight for carbon (C), nitrogen (N) and stable isotope (^{13}C and ^{15}N) analyses. Individual pyrosomes were treated similarly to the size-fractioned samples by first measuring total WW and dividing the WW into subsamples for pigment, DW and CN analyses.

CN subsamples were weighed in small tin boats, packed into pellets, and analyzed by standard elemental analyzer, isotope ratio mass spectrometry (EA-IRMS) (Owens and Rees, 1989) at the Isotope Biogeochemistry lab at Scripps Institution of Oceanography. The continuous flow system consisted of a Perkin Elmer CHN analyzer coupled to a Thermo/Finnigan Delta Plus IRMS. Acetanilide was the standard used for measurement stability on every run. C and N biomass estimates (mg m^{-2}) were computed for each size fraction from C:DW and N:DW ratios. Stable isotope values are reported in standard δ (‰) notation relative to atmospheric N_2 and Vienna Pee Dee Belemnite for carbon.

Gut pigment and grazing estimates

WW subsamples were placed in glass tubes with 7 mL of 90% acetone and homogenized (multiple 20-s bursts) in an ice bath with a Vibracell sonicator probe. They were then extracted overnight (18–24 h) in a −20°C freezer and warmed to room temperature in a dark container prior to analysis. The homogenate was shaken and centrifuged (5 min at 3000 rpm) to remove particulates. Concentrations of chlorophyll *a* (Chl*a*) and phaeopigments (Phaeo) were then measured by the acidification method using a 10-AU fluorometer (Strickland and Parsons 1972). Water-column estimates of depth-integrated Chl*a* for the euphotic zone were made similarly from analyses of duplicate 0.25 L samples collected from CTD hydrocasts, extracted for 24 h in 90% acetone, and measured on the same fluorometer.

For each size-fraction analyzed, we computed the depth-integrated concentration of gut pigment (Chl*a*, Phaeo) in the euphotic zone as:

$$\mathrm{GPC} = \frac{\mathrm{pig}^{*}D}{\mathrm{vol}^{*}f}$$

where GPC is gut pigment content (mg m^{-2}), pig is the measured pigment value (mg), f is fraction of sample analyzed, D is depth of tow (m) and vol is the volume of water filtered (m^3). To be conservative, our zooplankton grazing estimates are based only on measured gut Phaeo values, without correction for inefficiencies in converting Chl*a* into Phaeo.

We estimated grazing rates (G, mg pigment m^{-2} $time^{-1}$) for each size fraction and for the total zooplankton assemblage as $G = GPC * K$, where K (min^{-1}) is the gut evacuation rate constant. For K, we used a gut passage rate of 2.1 h^{-1} measured under similar surface water temperatures in the equatorial Pacific (Zhang *et al.*, 1995). To compute carbon-specific rates of phytoplankton grazing by the zooplankton size classes, we divided G by carbon biomass (mg C m^{-2}). Daily removal rates of phytoplankton by zooplankton grazing were computed as $G * Chl_z^{-1}$, where Chl_z is the depth-integrated concentration of Chl*a* in the euphotic zone (mg Chl*a* m^{-2}).

Carnivorous feeders

As a relatively simple index of trophic structure, we divided the mesozooplankton community into two feeding groups: animals considered to be exclusively carnivorous (only consuming other animals) and omnivorous suspension feeders (mixed feeding on phytoplankton, suspended particles, heterotrophic protists and likely small developmental stages of other animals). For this, we volumetrically subsampled the formalin-preserved split of the zooplankton samples with a Stempel pipette after thorough mixing and size fractioned the sample through a 1-mm Nitex screen. Except for C2, 2-day and 2-night tows were subsampled from each cycle. After rinsing with fresh water, zooplankton taxa in the > 1-mm fraction were identified under a dissecting microscope and sorted into carnivores and suspension feeders. Each group was placed together on pre-weighed Nitex, dried for 24 h at 60°C and measured as DW. Percent carnivore was determined as the fraction of total subsample DW attributable to carnivorous taxa. For the < 1-mm fraction, we determined percent carnivore in terms of relative abundances by dispersing the subsample in a Bogorov sorting tray and enumerating the first ~275 animals encountered (range 255–316) into the two feeding categories.

Metabolic and growth requirements

To estimate feeding requirements for well-nourished zooplankton, we calculated expected rates of respiration and growth from empirical relations based on zooplankton size and environmental temperature. For respiration, we used the equation of Ikeda (1985):

$$\ln R_o\left(\mu l\ O_2\ ind^{-1}\ h^{-1}\right) = 0.8354 * \ln C_i\left(mg\ C\ ind^{-1}\right) + 0.0601 * T\ (°C) + 0.5254,$$

where C_i is the average carbon content of an individual zooplankter in size-fraction i. Potential growth rates (G, d^{-1}) were computed from the equation of Hirst and Sheader (1997):

$$\log_{10} G\ \left(d^{-1}\right) = -0.2962 * \log_{10} C_i\left(\mu g\ C\ ind^{-1}\right) + 0.0246 * T\ (°C) - 1.1355.$$

For both respiration and growth rate equations, we used mean estimates of individual zooplankton carbon (2.4, 7.4, 41, 140 and 2 782 μg C ind^{-1} for the 0.2–0.5 to 5+ mm size fractions, respectively) determined from measured size-fractioned abundances and carbon biomass in 144 net tows from the subtropical Pacific (Landry *et al.*, 2001). Temperature was the mean euphotic-zone value (T_{EZ}) in Table I. Respiration rates for each size class were converted to carbon equivalents using the molar volume of an ideal gas at standard temperature and pressure (22.4 L mol^{-1}), the respiratory quotient (0.97; Hernández-León and Ikeda, 2005), and the molecular weight of carbon (12 g C mol^{-1}) and multiplying by zooplankton abundance (total C biomass/C ind^{-1}). Growth rates (d^{-1}) were converted to production estimates by multiplying by C biomass of the zooplankton assemblage (mg C m^{-2}) and averaging day and night estimates at each station. Calculations of ingestion rates (carbon demand) needed to satisfy respiration and growth requirements also assumed 70% absorption efficiency for ingested food (Steinberg and Landry, 2017). Estimates of mesozooplankton contribution to carbon export by active diel vertical migrators were similarly calculated from the biomass differences between paired day and night tows (size-fractioned migrant biomass) and the mean temperature in the 300–500-m depth range assuming that migrants spend 12 h per day in this stratum (Al Mutairi and Landry, 2001).

RESULTS

Environmental conditions

All zooplankton net tows were conducted in warm oligotrophic waters with low mixed-layer Chl*a* and prominent deep chlorophyll maxima (DCM). Mixed-layer depths (MLD) were generally in the range of 20–35 m but substantially deeper and more variable for T1 sampling (56 ± 17 m) and shallowest (12 ± 0.5 m) for C5 (Table I). DCM depths varied by > 40 m on each cruise but were 22-m shallower, on average, during 2018 compared with 2017 ($p < 0.001$). Conversely, integrated concentrations of euphotic-zone Chl*a* were higher in 2018 than in 2017 for all composite sampling locations, and almost double on average ($p < 0.001$). While mixed-layer Chl*a* varied slightly, but significantly for 2017 and 2018 (0.11 ± 0.01 versus 0.09 ± 0.01 mg Chl*a* m^{-3}, respectively; $p < 0.004$), most of the difference between years was in the lower euphotic zone, as indicated by larger DCM peak concentrations in 2018 (0.71 ± 0.04 versus 0.54 ± 0.04 mg Chl*a*

Table I: Environmental conditions for zooplankton net tows in the GoM during May 2017 (Cycles 1–3) and April–May 2018 (Transects 1–2; Cycles 4–5)

Samples	Dates	MLD (m)	DCM (m)	T_{ML} (°C)	T_{EZ} (°C)	Chl*a* (mg m^{-2})
Cycle 1	11–14 May	31.5 ± 4.0	100 ± 1.3	24.5 ± 0.12	23.6 ± 0.36	17.7 ± 1.0
Cycle 2	16–18 May	24.2 ± 1.1	120 ± 7.9	25.3 ± 0.06	24.4 ± 0.04	16.2 ± 1.4
Cycle 3	27–30 May	25.8 ± 4.1	137 ± 1.7	26.7 ± 0.07	24.8 ± 0.02	13.7 ± 0.7
Trans 1	30 Apr–1 May	56.1 ± 17.2	100 ± 10.8	26.1 ± 0.28	25.2 ± 0.77	35.1 ± 6.7
Trans 2	2 May	26.6 ± 0.4	92 ± 4.4	24.9 ± 0.10	24.2 ± 0.49	43.0 ± 0.3
Cycle 4	5–9 May	23.7 ± 1.2	111± 7.1	25.6 ± 0.07	24.8 ± 0.05	24.1 ± 1.2
Cycle 5	15–19 May	12.4 ± 0.5	77 ± 3.9	25.5 ± 0.14	24.2 ± 0.22	29.2 ± 5.4
2017		**28.1 ± 1.6**	**118 ± 4.0**	**25.5 ± 0.23**	**24.2 ± 0.15**	**15.8 ± 0.5**
2018		**26.4 ± 5.0**	**95 ± 4.6**	**25.6 ± 0.10**	**24.5 ± 0.20**	**29.4 ± 2.3**

MLD (m) = mixed layer depth, where seawater density is 0.1 kg m^{-3} greater than at 10 m. DCM (m) = depth of the Deep Chlorophyll Maximum; T_{ML} (°C) = mean temperature of the mixed layer; T_{EZ} (°C) = mean euphotic-zone temperature to the DCM; and CHL_Z (mg m^{-2}) is mean depth-integrated Chl*a* to the DCM. 2017 and 2018 cruise are averages for all tows in cruise years. Uncertainties are standard errors of mean values.
Bold font is used to highlight the averages of cruise years, as opposed to the averages of individual cycle experiments in the two years.

Table II: Carbon (C), nitrogen (N), WW and DW relationships for mesozooplankton size classes in the oceanic GoM

Size fraction	DW:WW (%)	C:DW (%)	N:DW (%)	C:N
0.2–0.5 mm	14.8 ± 0.8	36.8 ± 0.3	8.18 ± 0.09	4.51 ± 0.03
0.5–1 mm	16.5 ± 1.0	39.4 ± 0.3	9.91 ± 0.08	4.28 ± 0.02
1–2 mm	11.6 ± 0.4	38.5 ± 0.3	9.06 ± 0.08	4.25 ± 0.03
2–5 mm	13.4 ± 1.8	35.7 ± 0.4	8.61 ± 0.11	4.15 ± 0.04
5+ mm	8.5 ± 2.0	26.5 ± 1.6	6.21 ± 0.45	4.21 ± 0.16
Total	**12.1 ± 0.7**	**36.0 ± 1.6**	**8.47 ± 0.14**	**4.25 ± 0.03**

Averages are based on 44 day and nighttime euphotic-zone net tows in May 2017 and May 2018. Uncertainties are standard errors of mean values.
Bold font is used to highlight the averages of cruise years, as opposed to the averages of individual cycle experiments in the two years.

m^{-3}; $p < 0.001$). Despite the Chl*a* differences, water temperatures varied narrowly ~24.5–26.5°C for the mixed layer and 23–25°C for the euphotic zone and were not different, on average, between years ($p > 0.20$).

Elemental and weight relationships

Day-night differences in DW:WW ratios were not significant for any of the zooplankton size classes ($P > 0.25$). In 2017, C:DW was significantly lower at night (33.4 ± 1.9%) than during the day (38.4 ± 0.6%) due to more large gelatinous animals in the euphotic zone at night, which lowered the carbon content of the 5+ mm size fraction from 30.6 to 19.1% of DW ($P < 0.035$). For 2018 and the other 2017 size fractions, day-night variability in %C:DW was insignificant. Because most of the variability in elemental and weight conversions occurs among size classes rather than time of day, we highlight these differences by averaging all day and night tows together in Table II.

Carbon is the biomass basis for all subsequent analyses. The C:DW relationship is highest for the 0.5–1 and 1–2 mm fractions (39.4 and 38.5%, respectively) and decreases significantly in the order of 0.2–0.5 mm (36.8%; $P < 0.001$) > 2–5 mm (35.7%; $P < 0.05$) > 5+ mm (26.5%; $P < 0.001$; Table II). The C:N ratio for the 0.2–0.5 mm fraction (4.51) is significantly higher than both of the 1–2 and 2–5 mm fractions (4.25 and 4.15, respectively; $P < 0.0001$), while all other size fractions show no C:N differences. The difference in the smallest size fraction may reflect some contamination from large phytoplankton or detritus, which have higher C:N compositions than zooplankton.

Biomass variability

Mesozooplankton carbon biomass varies substantially in our analyses among sampling locations (cycles), between day-night tows, between cruise years and among size classes (Fig. 2). Among cycles, mean day biomasses range 5 fold from 101 ± 12 to 513 ± 71 mg C m^{-2} for C2 and C5, respectively. Nighttime biomasses range 3.7 fold from 216 ± 16 (C1) to 798 ± 28 (C5) mg C m^{-2}. Within years, night tow biomass averages are significantly higher than day averages in 2017 (239 ± 15 versus 144 ± 16 mg C m^{-2}; $P < 0.001$), but not in 2018 (514 ± 69 versus 424 ± 53 mg C m^{-2}; $P > 0.31$). Between years, both day and night biomass

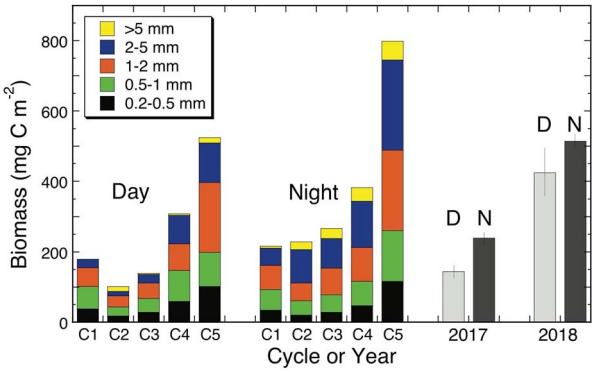

Fig. 2. Size-fractioned carbon biomass structure of mesozooplankton in the GoM during Cycles 1–5 drift experiments and total average carbon for day (D) and night (N) tows in 2017 and 2018 cruises. Totals for 2018 include T1 and T2 sampling, in addition to C4 and C5. Uncertainties are standard errors of mean estimates.

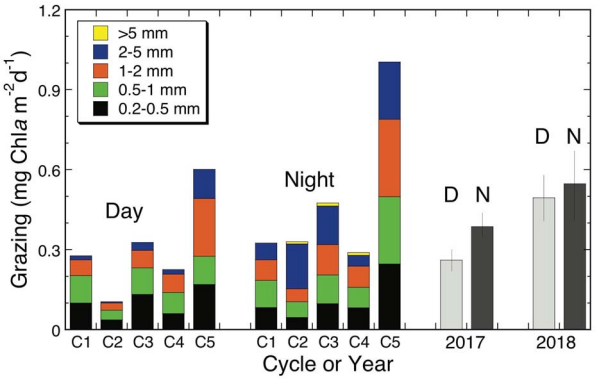

Fig. 3. Size-fractioned grazing of mesozooplankton in the GoM during Cycles 1–5 drift experiments and average total grazing for day (D) and night (N) tows in 2017 and 2018 cruises. Uncertainties are standard errors of mean estimates.

averages are significantly higher in 2018 than 2017 for the total ($P < 0.002$) and for each individual size fraction in day and night tows ($P < 0.02$), except for 5+ mm animals during the day ($P > 0.40$). Among size classes for all net tows, the 1–2 mm fraction contributes most to biomass ($29.9 \pm 1.3\%$; $P < 0.016$), the 0.5–1 and 2–5 mm fractions contribute comparably (23.7 ± 1.2 and $24.8 \pm 1.6\%$, respectively; $P > 0.60$), and further contributions decline in order of 0.2–0.5 mm ($16.5 \pm 0.9\%$; $P < 0.001$) and 5+ mm fractions ($5.0 \pm 0.8\%$; $P < 0.001$). For night tows only, inclusive of diel migrants, the 2–5 and 1–2 mm fractions are the biomass co-dominants (29.1 ± 2.1 and $27.4 \pm 1.7\%$, respectively; $P > 0.54$), and further contributions decline in order of 0.5–1 mm ($22.2 \pm 1.6\%$; $P < 0.03$), 0.2–0.5 mm ($14.2 \pm 1.1\%$; $P < 0.001$) and 5+ mm fractions ($7.2 \pm 1.2\%$; $P < 0.001$).

Grazing rates and size relationships

Mean grazing rate estimates range from 0.1 to 1.0 mg Chl*a* m^{-2} d^{-1} for the whole mesozooplankton community and show substantial variability among cycles, day and night tows, years and size classes (Fig. 3). The main differences are shaped by the variability in biomass (Fig. 2). Similar to biomass trends, for example, the lowest and highest grazing rates are for C2 and C5 (0.22 ± 0.08 and 0.82 ± 0.13 mg Chl*a* m^{-2} d^{-1}, respectively; $P < 0.004$), and 2018 grazing is higher overall compared with 2017 (0.52 ± 0.08 and 0.33 ± 0.03 mg Chl*a* m^{-2} d^{-1}; $P < 0.025$). In contrast to biomass, however, nighttime grazing estimates do not differ significantly from day estimates for the full community for either of the 2 years separately or both years combined (0.48 ± 0.07 versus 0.39 ± 0.06 mg Chl*a* m^{-2} d^{-1}, $P > 0.38$), and only the 2–5 mm fraction has a marginal difference between night and day tows ($P < 0.048$). These departures from the biomass trends reflect differences among size classes and cycles in carbon-specific grazing rates (Table III).

Overall, we found no significant differences between day and night estimates of C-specific grazing for any of the size fractions ($P > 0.05$ for 5+ mm; $P > 0.21$ for all other sizes) or for the whole community ($P > 0.38$). C-specific grazing does, however, vary significantly among all size classes, as might be expected, in exact inverse order of mean animal size (Table III, $P < 0.03$:0.2–0.5 mm (2.43 ± 0.23μg Chl mg C d^{-1}) > 0.5–1 mm (1.65 ± 0.12 μg Chl mg C d^{-1}; $P < 0.003$) > 1–2 mm (1.14 ± 0.07 μg Chl mg C d^{-1}; $P < 0.001$) > 2–5 mm (0.85 ± 0.02 μg Chl mg C d^{-1}; $P < 0.03$) > 5+ mm (0.05 ± 0.02 μg Chl mg C d^{-1}; $P < 0.001$). Although C-specific grazing estimates are higher in 2017 than 2018 across all sizes (Table III), the differences are significant for only the 0.2–0.5 mm ($P < 0.004$), 2–5 mm ($P < 0.016$) and total ($P < 0.001$) size categories.

Isotopic composition

Day and night tows did not give statistically different isotopic values for any of the zooplankton size fractions and are reported as mean values in Fig. 5. δ^{15}N also did not differ among size fractions in the 2 years, but δ^{13}C was 0.3–0.6‰ lower ($P < 0.01$) for the smallest 3 fractions (0.2–2 mm) in 2018 compared with 2017. Among size classes, δ^{15}N increases significantly from 0.2–0.5 mm (3.38 ± 0.19‰) to 0.5–1 mm (4.05 ± 0.19‰; $P < 0.014$) and to 1–2 mm (4.96 ± 0.22‰; $P < 0.003$) zooplankton, but size fractions > 1 mm have similar values in the range of 5.0–5.25‰ ($P > 0.35$) (Fig. 5A). Assuming that a 3.4‰ increase in bulk δ^{15}N corresponds to one full trophic level

Table III: Carbon-specific grazing rates for size-fractioned mesozooplankton in the GoM during Cycle 1–5 experiments and for all tows in 2017 and 2018 cruises

	Carbon-specific grazing rates (μg Chl*a* mg C^{-1} d^{-1})					
Samples	0.2–0.5 mm	0.5–1 mm	1–2 mm	2–5 mm	5+ mm	Total
Cycle 1	2.51 ± 0.22	1.68 ± 0.18	1.06 ± 0.15	0.85 ± 0.27	—	1.50 ± 0.13
Cycle 2	2.19 ± 0.07	1.45 ± 0.14	0.81 ± 0.18	1.05 ± 0.45	0.14 ± 0.14	1.22 ± 0.12
Cycle 3	4.25 ± 0.64	2.28 ± 0.17	1.53 ± 0.13	1.50 ± 0.33	0.12 ± 0.08	2.06 ± 0.17
Cycle 4	1.67 ± 0.32	1.09 ± 0.11	0.90 ± 0.09	0.39 ± 0.11	0.06 ± 0.06	0.81 ± 0.11
Cycle 5	2.04 ± 0.31	1.84 ± 0.39	1.35 ± 0.22	0.88 ± 0.18	0.001 ± 0.001	1.24 ± 0.15
2017	**3.18 ± 0.35**	**1.88 ± 0.13**	**1.20 ± 0.10**	**1.17 ± 0.20**	**0.08 ± 0.04**	**1.67 ± 0.12**
2018	**1.86 ± 0.26**	**1.47 ± 0.17**	**1.09 ± 0.10**	**0.61 ± 0.09**	**0.03 ± 0.20**	**1.05 ± 0.09**

Uncertainties are standard errors of mean values.
Bold font is used to highlight the averages of cruise years, as opposed to the averages of individual cycle experiments in the two years.

of isotopic enrichment (Minawaga and Wada, 1984), the 1.87‰ difference between smaller and larger zooplankton size fractions suggests a 0.55 step increase in mean trophic position.

Despite the slight negative trend, none of the size-fraction comparisons for $\delta^{13}C$ are significant ($P > 0.35$; Fig. 5B). On average, therefore, zooplankton in the different size classes appears to share a common food-web base.

Carnivorous feeders

Among smaller (0.2–1 mm) mesozooplankton, carnivorous taxa comprised a small, but relatively consistent, fraction of the community (13.1 ± 0.7%) that did not vary significantly ($P > 0.07$) between day and night sample collections (Fig. 5). Copepods of the family Corycaeidae and small chaetognaths were the main contributors to this feeding group in the samples examined.

Among larger (>1 mm) zooplankton, carnivorous taxa dominated euphotic-zone biomass, significantly more during day (78.4 ± 5.0%) than night tows (60.5 ± 4.5%; $P < 0.013$) (Fig. 5). This difference reflects the entry of diel vertical migrants into the euphotic zone at night, especially large euphausiids, which we scored conservatively as omnivorous suspension feeders given the undocumented feeding status of most species. Conspicuous taxa comprising the carnivorous group were abundant large chaetognaths and large copepods of the genus *Euchaeta*, most of which appeared to reside in the euphotic-zone day and night. In addition to euphausiids, copepods of the genera *Neocalanus* and *Eucalanus* were significant contributors to suspension feeding biomass in most samples, while salps were relatively small and rare. This analysis does not account for the pyrosomes removed from samples prior to splitting, which were few in number (5 small colonies in 44 tows) and only collected at night. Considering pyrosomes would therefore have lowered the nighttime percentage of carnivorous biomass, though not substantially.

Carbon demand and migrant export

Because temperature varies little among the sampling locations (Table I), calculated estimates of mesozooplankton carbon demand (Fig. 6) closely follow biomass variability (Fig. 2), except that smaller size classes contribute proportionally more to total C demand because of the size functions in respiration and growth equations (Ikeda, 1985; Hirst and Sheader, 1997). C demand ranges from 67.5 ± 0.5 to 15.1 ± 0.1% body C d^{-1} for 0.2–0.5 mm and 5+ mm size fractions, respectively, and averages 42 ± 0.7% body C d^{-1} for the community. Day-night and cruise differences of C demand as % body C d^{-1} are insignificant. The total feeding required to meet C demand is, however, significantly higher in 2018 than 2017 (194 ± 17 versus 80 ± 6 mg C m^{-2} d^{-1}; $P < 0.001$).

The annual averages in Fig. 6 separate portions of total C demand that can be satisfied by carnivorous versus omnivorous suspension feeding based on the contributions of those feeding groups to small (0.2–1 mm) and large (>1 mm) zooplankton in Fig. 5. The proportions of C demand assigned to each feeding group were partitioned according to average % carnivore for day and night tows of each cycle (T1 and T2 samples were portioned according to mean day and night estimates for C4 and C5 combined), then summed for the total community and averaged per year. Of the total C demand for 2017, 29.1 ± 2.1 and 50.4 ± 4.0 mg C m^{-2} d^{-1} are ascribed to carnivores and suspension feeders, respectively. For 2018, C demand divides into 74.9 ± 7.0 and 119.2 ± 10.8 mg C m^{-2} d^{-1} for carnivores and suspension feeders. On average, ~38% of total C demand can be satisfied by direct predation on metazooplankton.

Mean temperature in the 300–500 m depth stratum ranged from 10.6 to 12.4°C (11.7 ± 0.02°C) for the 5 cycles where we had paired day and night tows to compute active export flux by respiration of diel migrants. Some of the estimates were slightly negative when day biomass values exceeded nighttime values (range − 3.3 to

15.6 mg C m^{-2} d^{-1}). The mean active export estimate of 3.7 ± 1.1 mg C m^{-2} d^{-1} represents, on average, the daily respiratory loss of $3.2 \pm 0.4\%$ of the body C of migrant zooplankton.

DISCUSSION

Although we intended to sample consistently in this study to depths that included the DCM, that was not possible for all tows on the 2017 cruise. Because DCMs were deepest for C2 and C3, the samples collected for those cycles were the most compromised by this issue, with missed DCM sampling potentially affecting estimates of total biomass m^{-2}, day-night differences, relative size structure and grazing rates relative to water-column Chl*a*. For example, the daytime biomass estimates for C2 and C3 are the lowest for all tows while nighttime estimates are comparable or higher than for C1 (Fig. 2). Similarly, daytime grazing estimates are extremely low for C2, though not for C3, whereas nighttime grazing for C2 and C3 are both comparable and higher than C1 and C4 (Fig. 3). A substantial portion of the zooplankton community appears to reside in the lower euphotic zone, between 100 m and the DCM, during the day, but comes into the upper 100 m at night, along with regular migrants that completely leave the euphotic zone during the day. Thus, while C2 and C3 euphotic depths were undersampled also at night, nighttime biomass and grazing estimates to 100 m provide more useful comparisons to other cycles. Based on them, the biomass difference between years appears to be valid, scaling approximately with the 2-fold higher concentrations of integrated Chl*a* in 2018 compared with 2017 (Table I). Grazing, however, does not scale proportionately with the Chl*a* difference between years because the C-specific grazing rate for the zooplankton community was ~60% higher in 2017 (Table III).

Due to the sampling depth irregularities for C2 and C3, we focus most of the discussion below on C1, C4 and C5, which are also the better characterized experiments for phytoplankton growth rates and microzooplankton grazing (Landry *et al*., this issue), allowing more comprehensive assessments of trophic interactions for these cycles. In the sections below, we first compare results for the GoM to other warm-water oceanic regions investigated with similar methods. We then address the two major questions of our study. What is the role of mesozooplankton grazing in the balance of phytoplankton growth and losses in the GoM? How do various trophic processes contribute to satisfying mesozooplankton carbon demand?

Comparisons to other open-ocean regions

Despite numerous corrections for net type, mesh size, tow depth and measurement units, global analyses have been useful in defining broad-scale patterns of zooplankton biomass (Moriarty and O'Brien, 2013; Moriarty *et al*., 2013). In general, subtropical waters (15–40°) are biomass minima between higher zooplankton stocks in tropical (15°S–15°N) and temperate-to-high-latitude (40–90°) waters. We examine the low-latitude, warm-water component of this pattern in Table IV for a subset of studies with methods comparable to the present study, including time-series sampling in the subtropical North Pacific (Stn. ALOHA, Hawaii Ocean Time-series, HOT) and subtropical North Atlantic (Sargasso Sea, Bermuda Atlantic Time-series Study, BATS) as well as process studies in the eastern tropical Pacific, equatorial Pacific and eastern Indian Ocean.

As in the global trend, mesozooplankton biomass is higher in our subset of studies for tropical regions than adjacent subtropical systems (Table IV). For example, biomass in the central equatorial Pacific (994 ± 77 mg C m^{-2}; Décima *et al*., 2011) is almost three times higher than the long-term average at Stn. ALOHA in the North Pacific subtropical gyre (349 ± 26 mg C m^{-2}; Valencia *et al*., 2018). Biomass in tropical waters of the eastern Indian Ocean along 110°E is also more than double the average in subtropical Indian Ocean Central Water directly to the south (455 ± 18 versus 209 ± 32 mg C m^{-2}; Landry *et al*., 2020a). Similarly, various crossing of the Atlantic Meridional Transect have documented substantially higher (1.5-16X) zooplankton biomass in the equatorial Atlantic than in subtropical gyres of the North and South Atlantic (Isla *et al*., 2004; López and Anadón, 2008; Calbet *et al*., 2009). Such differences arise because these tropical systems are associated with divergence or mixing centers that enhance productivity relative to the more pervasive downwelling of subtropical gyres. Nonetheless, as shown in Table IV, this occurs without much of a difference in total integrated Chl*a* because the shallow concentrated euphotic zones of richer systems are compensated for by deeper euphotic zones with pronounced DCMs in the subtropics. The importance of relative productivity, rather than latitude, in driving such differences is illustrated by sampling along 160°E in the western Pacific (Sun and Wang, 2017). In this case, equatorial waters are a local minimum in mesozooplankton biomass compared with the latitudinal trend to the north because they reside in a deep layer of oligotrophic waters, the Western Warm Pool, which does not allow significant upwelling of nutrients despite conducive winds.

GoM results are consistent with the lower primary production and zooplankton biomass expected for subtropical regions (Table IV). Our mesozooplankton biomass estimates are almost identical to the long-term average from the subtropical Pacific at Stn. ALOHA (349 versus 351 mg C m^{-2}, respectively), though substantially

Table IV: Comparison of environmental conditions, mesozooplankton biomass and grazing estimates among open-ocean tropical and subtropical regions

Region	Latitude	T_{EZ} (°C)	Intgr Chla (mg m^{-2})	PrimProd (mg C m^{-2} d^{-1})	Biomass (mg C m^{-2})	Grazing (% Chl*a* d^{-1})	Refs
Costa Rica Dome	9–11 °N	22.0 ± 0.3	24.1 ± 1.5	1 025 ± 113	1870 ± 72	54 ± 11	1
Equatorial Pacific	4°S-4°N	24.2 ± 0.2	26.7 ± 0.7	672 ± 3.7	994 ± 77	14 ± 6	2
Tropical E. Indian	11–14°S	26.9 ± 0.6	25.7 ± 2.9	ND	455 ± 18	21 ± 4	3
Subtrop. E. Indian	27–35°S	19.6 ± 0.4	27.2 ± 3.8	ND	209 ± 32	3 ± 0.4	3
W. Equat. Pac, 160°E	5°S–10°N	30.0	25.5	ND	259	ND	4
Subtrop. N. Pacific	22–23°N	24.4 ± 0.1	23.0 ± 0.2	516 ± 11	349 ± 26	ND	5
Subtrop. Atlantic	31–32°N	21.3 ± 0.1	24.8 ± 2.4	455 ± 11	218 ± 4	3 to 24	6
Gulf of Mexico	25.4–27°N	24.5 ± 0.2	22.8 ± 0.2	325 ± 14	351 ± 33	2 ± 0.2	7

References: (1) Décima *et al*. (2016), Landry *et al*. (2016), Taylor *et al*. (2016); (2) Balch *et al*. (2011), Décima et al. (2011), Landry *et al*. (2011), Taylor *et al*. (2011); (3) Landry *et al*. (2020b); (4) Sun and Wang (2017); (5) Hawaii Ocean Time series (HOT), https://hahana.soest.hawaii.edu/hot/hot-dogs/, Valencia *et al*. (2018); (6) Bermuda Atlantic Time Series (BATS), http://bats.bios.edu/data/, Madin *et al*. (2001), Roman *et al*. (1993); (7) This study, Selph *et al*. (in press), Yingling *et al*. (this issue).

T_{EZ} (°C) and Intgr Chl*a* (mg m^{-2}) are mean temperature and depth-integrated Chl*a* of the euphotic zone. PrimProd is the measured rate of daily primary production from ^{14}C or ^{13}C-labeled bicarbonate uptake (mg C m^{-2} d^{-1}). Biomass (mg C m^{-2}) estimates are for mesozooplankton collected in oblique tows with 200-µm mesh nets covering the euphotic zone, originally presented as carbon or calculated from DW using a C:DW ratio of 0.36. Grazing impact estimates are for the percent of total euphotic-zone Chl*a* (phytoplankton) cleared by mesozooplankton per day. Uncertainties are standard errors of mean values.

higher than the average for BATS in the Sargasso Sea (218 ± 4 mg C m^{-2}). Though sampled similarly, HOT zooplankton biomass has long been known to exceed that at BATS (Roman *et al*., 2002), and they remain consistently separated even as biomass has increased by 60–80% in both systems over the past three decades (Sheridan and Landry, 2004; Steinberg *et al*., 2012; Valencia *et al*., 2016). Although mean primary production is also higher at Stn. ALOHA (516 versus 455 mg C m^{-2} d^{-1}), the two sites have different biomass:production ratios of 0.68 (HOT) and 0.48 mg C (mg C)$^{-1}$ d^{-1} (BATS). Paradoxically, relatively high zooplankton biomass in the GoM is associated with low primary production (325 mg C m^{-2} d^{-1}; Yingling *et al*., this issue), giving a much higher biomass:production ratio (1.07 mg C (mg C)$^{-1}$ d^{-1}) than either HOT or BATS. One explanation for this difference is temporal aliasing, as the GoM samples were only collected in May of 2 years, while the time-series station averages are for all months over many years. May sampling may simply catch a seasonal imbalance in the magnitude of accumulated zooplankton relative to contemporaneous primary production. In addition, since our GoM sampling was site selective, rather than spatially random, the difference could reflect unique aspects of the mesoscale features where ABT larvae are more abundant. Either way, during the ABT spawning peak in the GoM, the ratio of zooplankton biomass to primary production in the larval rearing area is substantially higher than would be predicted from the averages of well-studied oligotrophic subtropical regions of the oceans.

Along with the biomass differences, zooplankton grazing impacts on phytoplankton, measured similarly to this study, are higher in tropical regions (14–54% Chl*a* d^{-1}) compared with estimates (2–3% Chl*a* d^{-1}) from subtropical areas. In this regard, the lower estimate of 3% d^{-1} for the subtropical Atlantic is from a study by Roman et al. (1993) that compared zooplankton grazing during stable stratified conditions (August), which prevail for most of the year, to the peak of a late-winter overturn event (March–April), which gave the higher (24% d^{-1}) grazing impact. The phytoplankton bloom that develops from the upward mixing of deep nutrients is a regular feature of the seasonal dynamics of the Sargasso Sea that makes this region more like a tropical upwelling system for a small portion of the year, as the higher grazing estimate indicates. The extent to which similar seasonal events might also occur in the GoM is not known, although the regular passage of strong tropical storms and hurricanes through the region in late summer have the potential to generate strong mixing on local scales (Babin *et al*., 2004; Avila-Alonso *et al*., 2020). At least for May, the region was strongly stratified and consistent with other subtropical systems during stratified conditions in showing a relatively low grazing impact of mesozooplankton.

Several previous studies have commented upon the relative uniformity of biomass distribution across size classes < 5 mm in subtropical regions of the Atlantic, Pacific and Indian Oceans (Landry *et al*., 2001; Madin *et al*., 2001; Valencia *et al*., 2018; Landry *et al*., 2020a). In our GoM samples, however, biomass structure was tilted to larger sizes, with the 2–5 mm fraction averaging 27% of biomass compared with 16% for 0.2–0.5-mm animals, whereas these two fractions are similar (20–23%) in other regions. Larger size classes contribute more to diel vertical migration. Our estimates of carbon

respiration at depth by diel migrating zooplankton, 3.7 ± 1.1 mg C m^{-2} d^{-1}, are close to comparably calculated active flux rates for the subtropical Pacific (3.6 ± 0.4 mg C m^{-2} d^{-1}, Al-Mutairi and Landry, 2001; updated to 4.2 ± 0.2 mg C m^{-2} d^{-1}, Valencia *et al*., 2018) but substantially higher than estimates for the subtropical Atlantic (1.2 mg C m^{-2} d^{-1}, Steinberg *et al*., 2000). Steinberg et al. (2012) updated the earlier migrant flux estimates for BATS to account for the increase in time-series biomass but did not separate the carbon respiratory component from the total active export (4.1 ± 0.3) that included organic excretion and fecal pellet transport. Based on the multipliers applied, the updated estimate for BATS is 60% of that at Stn. ALOHA (Valencia et al., 2018), so about 2.5 mg C m^{-2} d^{-1} for daytime C respiration at depth. Therefore, consistent with the differences in total community biomass, the magnitude of active migrant flux in the oceanic GoM during May is more like the average for the subtropical North Pacific than the western subtropical North Atlantic.

Phytoplankton growth and grazing balances

In addition to mesozooplankton grazing rates, measured daily rate profiles of phytoplankton growth, microzooplankton grazing and net changes in ambient water-column Chl*a* from dilution experiments during the cycle experiments (Landry *et al*., this issue) enable a first-order analysis of phytoplankton growth rates and fates for the euphotic zone based on fluorometrically measured Chl*a* (Table V). C2 is excluded from this analysis because it was a 2-day experiment with only one resolved rate profile. Depth-integrated estimates of phytoplankton growth rates range from 0.25 to 0.59 d^{-1}, and microzooplankton grazing (0.10–0.42 d^{-1}) is the major loss term compared with mesozooplankton grazing impact (0.01–0.03 d^{-1}). Net change in photic zone Chl*a* varies from a net accumulation rate of $+0.16$ d^{-1} for C5 to Chl*a* loss of -0.06 d^{-1} for C3. None of the water columns investigated was at steady state. For cycles where we observed net Chl*a* accumulation in the photic zone (C1, C4 and C5; Landry *et al*., this issue), the budgets can be reasonably closed, between -0.04 and $+0.09$ d^{-1}. Due to the net decline in Chl*a* during C3, a large portion of that balance (0.16 d^{-1}) is unresolved. Thus, for individual cycles, there is mixed success in reconciling the balance of growth and loss terms. For the daily resolved rates of all 4 cycles, the balance residual (0.05 ± 0.04 d^{-1}) is equivalent to $\sim 10\%$ of mean phytoplankton growth rate but is not significantly greater than zero (*t*-test, $P > 0.11$).

Similar analyses have demonstrated tighter balances of phytoplankton growth rates and fates in the California Current Ecosystem (Landry *et al*., 2009), equatorial Pacific (Landry *et al*., 2011) and Costa Rica Dome (Landry *et al*., 2016). In the California Current, measured rates of phytoplankton growth, microzooplankton grazing and mesozooplankton grazing explained 93% of the variability in rates of phytoplankton biomass accumulation along a trophic gradient from coastal upwelling to oligotrophic open ocean. In the equatorial Pacific and Costa Rica Domes, the dynamics were reflected in steady-state balances of growth and grazing with low to negligible unresolved residuals. What these previously studied systems have in common are phytoplankton concentration maxima in or close to the mixed layer, therefore in the depth stratum tracked by drifters with mixed-layer drogues. For the current experiments, Landry *et al*. (this issue) observed near steady-state mixed-layer Chl*a*, with microzooplankton grazing typically equal or exceeding phytoplankton growth, while growth and grazing were strongly uncoupled in the mid to lower photic zone, accounting for the net changes in ambient Chl*a*. Thus, a major challenge in interpreting growth-grazing balances in the GoM is the large influence of the portion of the photic zone that shows significant net biomass rate of change but is not specifically marked or tracked by the drifter. It is thus difficult to know whether imbalances for the cycles in Table V are due to process measurement issues versus lateral inputs that are not independently measured. Advective influences on water-column dynamics might also be exacerbated in the oceanic GoM by strong gradients in the surrounding coastal margins (Kelly *et al*., in review) and by our experimental site selection in mesoscale features. Given these complications, it may be fortuitous that the process balances are as well resolved as they appear.

Trophic flows, trophic structure and carbon demand

Direct grazing on phytoplankton is typically too low to support full respiration and growth of mesozooplankton in open-ocean ecosystems (Dam *et al*., 1995; Calbet *et al*., 2009). Nonetheless, as recently demonstrated for the equatorial Pacific (Landry *et al*., 2020b), the broader network of trophic flows—including omnivorous feeding on microzooplankton, carnivory and detritivory—might still be able to meet the carbon demands of active zooplankton computed from empirical relationships (Fig. 6). In Table VI, we evaluate this potential for the GoM for the three experimental cycles with adequate data for carbon fluxes. Carbon-based estimates of phytoplankton grazing (7–20 mg C m^{-2} d^{-1}), from daily mean day-night values of % Chl*a* d^{-1} cleared by mesozooplankton and phytoplankton C values for the photic zone (Selph *et al*., in press), account for $\sim 23\%$ of total mesozooplankton C

Table V: Phytoplankton growth rates and fates during cycle process experiments in the GoM

Rate (d^{-1})	Cycle 1	Cycle 3	Cycle 4	Cycle 5	ALL
Phyto growth	0.44 ± 0.06	0.37 ± 0.07	0.59 ± 0.05	0.50 ± 0.06	0.49 ± 0.03
Microzoo graz	0.34 ± 0.09	0.24 ± 0.06	0.42 ± 0.09	0.35 ± 0.07	0.34 ± 0.04
Mesozoo graz	0.02 ± 0.004	0.03 ± 0.002	0.01 ± 0.001	0.03 ± 0.002	0.02 ± 0.002
Net change	0.09 ± 0.05	−0.06 ± 0.08	0.06 ± 0.03	0.16 ± 0.09	0.07 ± 0.04
Residual	**−0.0004 ± 0.01**	**0.17 ± 0.05**	**0.09 ± 0.08**	**−0.04 ± 0.10**	**0.05 ± 0.04**

Growth-grazing balance residuals are the differences between measured rate estimates for phytoplankton growth and the sum of losses to micro- and mesozooplankton grazing plus the net rate of biomass change in the euphotic zone during the cycle. All rates are measured by fluorometric Chl*a* and integrated for the photic zone for daily experiments (Landry *et al.*, this issue). Uncertainties are standard errors of mean values.
Bold font is used to highlight the averages of cruise years, as opposed to the averages of individual cycle experiments in the two years.

Table VI: Comparisons of nutritional resources relative to mesozooplankton carbon demand for experimental cycles in the GoM

Variable	Cycle 1	Cycle 4	Cycle 5
Nutritional resource (mg C m^{-2} d^{-1})			
Phytoplankton grazing	20 ± 6	7 ± 1	20 ± 3
Microzoo production	126 ± 35	116 ± 10	121 ± 10
Mesozoo production	26 ± 3	42 ± 5	77 ± 9
Carbon demand (mg C m^{-2} d^{-1})			
Suspension feeders	61 ± 8	91 ± 11	159 ± 24
Carnivorous feeders	27 ± 3	56 ± 8	106 ± 9

Phytoplankton grazing is calculated from % Chl*a* grazed d^{-1} and phytoplankton C biomass m^{-2}. Microzoo production is calculated from the combined C grazing rates of microzooplankton on phytoplankton and bacteria from Landry *et al.* (this issue), assuming a 30% gross growth efficiency. Mesozoo Production is computed as described from empirical equations of Hirst and Sheader (1997). Carbon Demands are computed for suspension feeders and carnivores as described for Fig. 6. All rates are mg C m^{-2} d^{-1}. Uncertainties are standard errors of mean values.

demand for C1 and much lower (5–8%) percentages for C4 and C5. In comparison, microzooplankton production (116–126 mg C m^{-2} d^{-1}), from daily integrated C-based grazing rates of microzooplankton on phytoplankton and bacteria (Landry *et al.*, this issue) and assuming a gross growth efficiency of 30% (Straile, 1997), is 6–17 times more important as a potential food resource than phytoplankton. For C1 and C4, the combined resources from phytoplankton and microzooplankton substantially exceed the estimated C demands of suspension feeders. For C5, the small deficit is within the margin of error for C demand. While flux distributions would be more complicated in an actual trophic network, for example involving small and large microzooplankton and some use of detritus (Landry *et al.*, 2020b), this simple analysis indicates that trophic flows from locally generated production in the oceanic GoM in May are adequate to meet the C demands of suspension feeders, with most coming from predation on microzooplankton.

From Table VI, the challenge for reconciling trophic fluxes in the GoM appears to be the availability of sufficient mesozooplankton production, here calculated from Hirst and Sheader (1997), to satisfy carnivores. Mesozooplankton production and carnivore C demand are balanced for C1, while C4 and C5 have production deficits of 25–27%. Carnivore C demand could be overestimated because it derives from a copepod-based growth relationship (Hirst and Sheader, 1997), whereas the GoM carnivore biomass is dominated by chaetognaths. Indeed, the multiple regression equation developed by Ikeda (2014) for respiration of diverse zooplankton communities has a negative coefficient, relative to copepods, for the contribution of chaetognaths compared with a positive coefficient for euphausiids. For our samples, overestimates of C demand for chaetognaths would be offset by underestimates for euphausiids. In addition, given our very conservative assumption of no carnivorous feeding by euphausiids and many other groups, we more likely underestimate total carnivore C demand. An advective subsidy would be another way to meet the zooplankton production shortfall.

Kelly *et al.* (in review) argue for the importance of a lateral advective organic input from the coastal margins to explain mass balance deficits of N export in the open-ocean GoM. Mechanistically, material pulled northward by the loop current from the productive Campeche Bank of the Yucatan Peninsula (Merino, 1997; Melo Gonzalez *et al.*, 2000) could persist as a subsidy in the bodies of long-lived animals. Studies in the Northern GoM have also documented evolving dynamics of phytoplankton

and zooplankton during transport in the Mississippi River plume that leave depleted phytoplankton and a surplus of zooplankton on the seaward end (Liu and Dagg, 2003; Liu *et al*., 2005), where they can be transported into the oceanic region by eddies. In the present study, backtracking of water parcels sampled during our Lagrangian experiments shows a strong connectivity to the slope margin region of the NE GoM several weeks prior to our sampling for the C1 and C5 experiments with abundant ABT larvae, but absent that connectivity for cycles C2–C3 without larvae (Gerard *et al*., this issue). This suggest that the NE slope margin may be both a hot spot of adult spawning activity and a source region of lateral organic enrichment to the larval ABT rearing habitat. It may not be coincidental that the cycle (C5, Fig. 1) closest to this area shows the greatest need for a lateral subsidy of zooplankton to satisfy C demands of carnivores while locally generated and balanced trophic fluxes are sufficient to meet C demands of both suspension feeders and carnivores for water parcel C1 in the central oceanic GoM. Shropshire *et al.* (this issue) have further surmised that a nutritional subsidy from advected zooplankton may be important for larval ABT survival and point to the shelf-slope margin as the optimal spawning areas for minimizing starvation and predation risks of early larvae.

Dorado *et al*. (2012) found no difference in $\delta^{13}C$ values for zooplankton collected in neritic versus oceanic waters in the northern GoM (both averaging −19.8 to -19.9 ± 0.9‰ SD), despite very substantial $\delta^{13}C$ differences in the POM from these two areas. Our similar values among size classes (Fig. 4) agree with their conclusion of a common marine-based carbon source for the region. In terms of trophic structure, the differences in percent carnivorous feeders between large and small zooplankton are consistent with the inference of a 0.5–0.6 trophic step increase from $\delta^{15}N$ isotopic enrichment (Figs. 4 and 5). Despite no difference in $\delta^{13}C$, Dorado *et al.* (2012) reported significantly higher $\delta^{15}N$ values for neritic versus oceanic zooplankton (5.5 ± 1.1 and 2.8 ± 1.4‰, respectively, for June and July collections), which they attributed to the lower isotopic values of production from nitrogen fixers in the oceanic region. Our biomass-weighted mean values of $\delta^{15}N$ from Fig. 4 are in the range of 4.5–4.7‰, so closer to the previous $\delta^{15}N$ values for coastal zooplankton. In addition, nitrogen isotope mass balances for our experimental cycles also revealed very little contribution from diazotrophy during the times of our cruises (Knapp *et al*., this issue). If these differences between our results and Dorado *et al*. (2012) are indicative of a recurrent seasonal pattern, they suggest a profound and rapid shift up in the contribution of N_2 fixation to biomass production as the ocean warms and further stratifies between May and July.

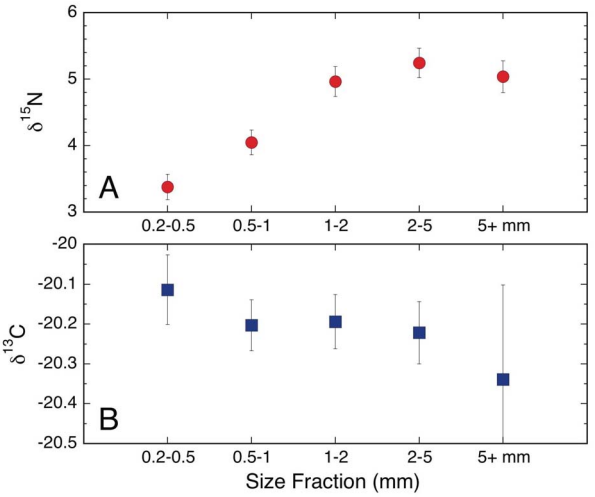

Fig. 4. Bulk $d^{15}N$ and $d^{13}C$ isotopic values for mesozooplankton size classes in the GoM. Uncertainties are standard errors of mean estimates.

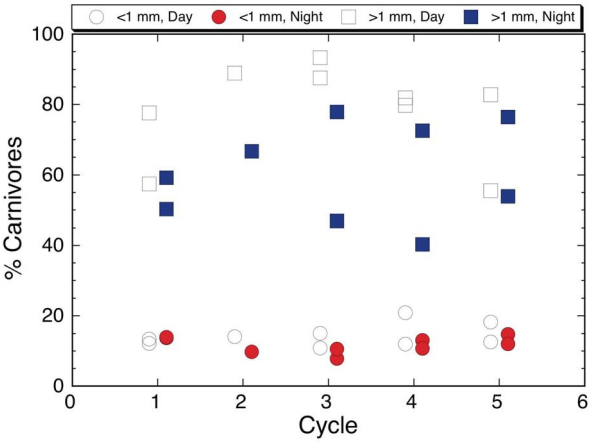

Fig. 5. Day and nighttime estimates of percent carnivorous mesozooplankton from net tows done during experimental cycles in the GoM. Estimates for the small (<1-mm) size fraction are based on relative abundances. Estimates for the large (>1-mm) size fraction are based on relative DW.

CONCLUSIONS

Despite a habitat bordered closely by land masses on almost all sides, mesozooplankton communities of the oceanic GoM exhibit generally similar characteristics to those of remote oligotrophic subtropical regions of the major oceans in terms of biomass, low grazing impact on phytoplankton and magnitude of active export from respiration by diel migrators. Compared with averages for HOT and BATS, however, zooplankton stocks are disproportionately high relative to contemporaneous primary production in the ABT larval rearing sites during the peak May season. Given the broader context of process experiments that measured trophic fluxes and net

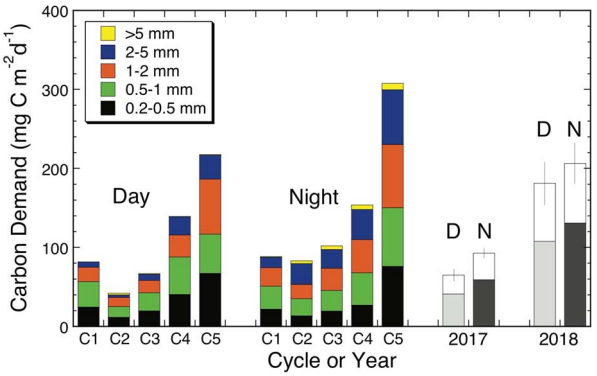

Fig. 6. Feeding requirements for mesozooplankton to meet carbon demands for respiration and production in the GoM during Cycles 1–5 experiments and the average day (D) and night (N) estimates for tows in 2017 and 2018. Yearly averages are divided into feeding requirements to support suspension feeders (gray-scale shaded, below) and requirements to support carnivorous feeders (unshaded, top). Uncertainties are standard errors of mean cruise estimates for the total community.

biomass changes in the ambient water column, growth-grazing balances for phytoplankton were resolved with a slight positive, but statistically insignificant, net residual, and trophic fluxes generated by local productivity were found sufficient to satisfy C demand of suspension feeders. Microzooplankton were the major contributors to these budgets. Other than the most remote experimental cycle, C1, which might be a model for how subtropical ocean regions operate as trophically balanced systems, experiments conducted closer to the GoM margin show a zooplankton production deficit, suggesting that lateral subsidy of zooplankton from the margins is important for meeting carnivore C demand in the open-ocean region.

DATA ARCHIVING

Data presented here have been submitted to the National Oceanic and Atmospheric Administration's (NOAA) National Centers for Environmental Information (NCEI) data repository and will also be archived at BCO-DMO (Biological and Chemical Oceanography Data Management Office) site https://www.bco-dmo.org/program/819631.

ACKNOWLEDGEMENTS

We gratefully acknowledge the capable leadership of John Lamkin and Trika Gerard for the project overall, the cruise Chief Scientists Estrella Malca (NF1704) and John Lamkin (NF1802), and the captain and crew of the R/V Nancy Foster. We additionally thank Sarah Privoznic for her assistance in organizing the cruises, and Cameron Quackenbush, Juan Banuelos-Arriaga, Kelsey Fleming and Tabitha Hernandez for assistance with the field collections and laboratory analyses.

FUNDING

This study acknowledges BLOOFINZ-GoM Program support from National Oceanic and Atmospheric Administration award NA15OAR4320071 and U.S. National Science Foundation grants OCE-1756517 and -1851558.

REFERENCES

Alemany, F., Quintanilla, L., Vélez-Belchí, P., García, A., Cortés, D., Rodríguez, J. M., DE Puelles, M. F., González-Pola, C. *et al.* (2010) Characterization of the spawning habitat of Atlantic bluefin tuna and related species in the Balearic Sea (western Mediterranean). *Prog. Oceanogr.*, **86**, 21–38.

Al-Mutairi, H. and Landry, M. R. (2001) Active export of carbon and nitrogen at station ALOHA by diel migrant zooplankton. *Deep-Sea Res. II.*, **48**, 2083–2104.

Avila-Alonso, D., Baetens, J. M., Cardenas, R. and De Baets, B. (2020) Oceanic response to hurricane Irma (2017) in the exclusive economic zone of Cuba and the eastern Gulf of Mexico. *Ocean Dynm.*, **70**, 603–619.

Babin, S. M., Carton, J. A., Dickey, T. D. and Wiggert, J. D. (2004) Satellite evidence of hurricane-induced phytoplankton blooms in an oceanic desert. *J. Geophys. Res., Oceans*, **109**. doi: 10.1029/2003JC001938.

Bakun, A. and Broad, K. (2003) Environmental 'loopholes' and fish population dynamics: comparative pattern recognition with focus on El Nino effects in the Pacific. *Fish. Oceanogr.*, **12**, 458–473.

Bakun, A. (2006) Fronts and eddies as key structures in the habitat of marine fish larvae: opportunity, adaptive response and competitive advantage. *Sci. Mar.*, **70**, 105–122.

Bakun, A. (2013) Ocean eddies, predator pits and bluefin tuna: implications of an inferred "low risk-limited payoff" reproductive scheme pf a (former) archetypical top predator. *Fish Fish.*, **14**, 424–438.

Balch, W. M., Poulton, A., Drapeau, D. T., Bowler, B. C., Windecker, L. A. and Booth, E. S. (2011) Zonal and meridional patterns of phytoplankton biomass and carbon fixation in the equatorial Pacific Ocean, between 110°W and 140°W. *Deep-Sea Res. II Top. Stud. Oceanogr.*, **58**, 400–416.

Calbet, A., Atienza, D., Henriksen, C. I., Saiz, E. and Adey, T. R. (2009) Zooplankton grazing in the Atlantic Ocean: a latitudinal study. *Deep-Sea Res II*, **56**, 954–963.

Cushing, D. H. (1990) Plankton production and yearclass strength in fish populations: an update of the match/mismatch hypothesis. *Adv. Mar. Biol.*, **26**, 249–293.

Dam, H. G., Zhang, X., Butler, M. and Roman, M. R. (1995) Mesozooplankton grazing and metabolism at the equator in the central Pacific: implications for carbon and nitrogen fluxes. *Deep-Sea Res II*, **42**, 735–756.

Décima, M., Landry, M. R. and Rykaczewski, R. (2011) Broad-scale patterns in mesozooplankton biomass and grazing in the eastern equatorial Pacific. *Deep-Sea Res. II Top. Stud. Oceanogr.*, **58**, 387–399.

Décima, M., Landry, M. R., Stukel, M. R., Lopez-Lopez, L. and Krause, J. W. (2016) Mesozooplankton biomass and grazing in the Costa Rica dome: amplifying variability through the plankton food web. *J. Plankton Res.*, **38**, 317–330.

Domingues, R., Goni, G., Bringas, F., Muhling, B., Lindo-Atichati, D. and Walter, J. (2016) Variability of preferred environmental

conditions for Atlantic bluefin tuna (*Thunnus thynnus*) larvae in the Gulf of Mexico during 1993-2011. *Fish. Oceanogr.*, **25**, 320–336.

Dorado, S., Rooker, J. R., Wissel, B. and Quigg, A. (2012) Isotope baseline shifts in pelagic food webs of the Gulf of Mexico. *Mar. Ecol. Prog. Ser.*, **464**, 37–49.

Gerard, T., Lamkin, R. T., Kelly, T. B., Knapp, A. N., Laiz-Carrión, R., Malca, E., Selph, K. E., Shiroza, A. *et al.* (this issue) Bluefin larvae in Oligotrophic Ocean Foodwebs, investigations of nutrients to zooplankton: overview of the BLOOFINZ-Gulf of Mexico program. *J. Plankton Res.*.

Hardy, A. C. (1924) The herring in relation to its animate environment, part I. the food and feeding habits of the herring with special reference to the east coast of England. *Fish. Invest. Lond. Ser. 2*, **7**, 1–53.

Hernández-León, S. and Ikeda, T. (2005) A global assessment of mesozooplankton respiration in the ocean. *J. Plankton Res.*, **27**, 153–158.

Hirst, A. G. and Sheader, M. (1997) Are in situ weight-specific growth rates body-size independent in marine planktonic copepods? A re-analysis of the global synthesis and a new empirical model. *Mar. Ecol. Prog. Ser.*, **154**, 155–165.

Hjort, J. (1914) Fluctuations in the great fisheries of northern Europe viewed in the light of biological research. *Rapp. P.-V. Réun. Cons. Int. Explor. Mer*, **20**, 1–228.

Ikeda, T. (1985) Metabolic rates of epipelagic marine zooplankton as a function of body size and temperature. *Mar. Biol.*, **85**, 1–11.

Ikeda, T. (2014) Respiration and ammonia excretion by marine metazooplankton taxa: synthesis toward a global-bathymetric model. *Mar. Biol.*, **161**, 2753–2766.

Isla, J. A., Llope, M. and Anadón, R. (2004) Size-fractionated mesozooplankton biomass, metabolism and grazing along a 50°N-30°S transect of the Atlantic Ocean. *J. Plankton Res.*, **26**, 1301–1313.

Kelly, T. B., Knapp, A. N., Landry, M. R., Selph, K. E., Shropshire, T. A., Thomas, R. and Stukel, M. R. (in review) Lateral advection supports nitrogen export in the oligotrophic open-ocean Gulf of Mexico. *Nat. Commun.*.

Kleppel, G. S. and Pieper, R. E. (1984) Phytoplankton pigments in the gut contents of planktonic copepods from coastal waters off Southern California. *Mar. Biol.*, **78**, 193–198.

Knapp, A. N., Thomas, R., Stukel, M. R., Kelly, T. B., Landry, M. R., Selph, K. E., Malca, E., Gerard, T. *et al.* (this issue) Constraining the sources of nitrogen fueling phytoplankton and food webs in the Gulf of Mexico using nitrogen isotope budgets. *J. Plankton Res.*.

Landry, M. R., Al-Mutairi, H., Selph, K. E., Christensen, S. and Nunnery, S. (2001) Seasonal patterns of mesozooplankton abundance and biomass at station ALOHA. *Deep-Sea Res. II*, **48**, 2037–2061.

Landry, M. R., Beckley, L. E. and Muhling, B. A. (2019) Climate sensitivities and uncertainties in food-web pathways supporting larval bluefin tuna in subtropical oligotrophic oceans. *ICES J. Mar. Sci.*, **76**, 359–369.

Landry, M. R., Hood, R. R. and Davies, C. H. (2020a) Mesozooplankton biomass and temperature-enhanced grazing along a 110°E transect in the eastern Indian Ocean. *Mar. Ecol. Prog. Ser.*, **649**, 1–19.

Landry, M. R., Ohman, M. D., Goericke, R., Stukel, M. R. and Tsyrkevich, K. (2009) Lagrangian studies of phytoplankton growth and grazing relationships in a coastal upwelling ecosystem off Southern California. *Prog. Oceanogr.*, **83**, 208–216.

Landry, M. R., Selph, K. E., Décima, M., Gutiérrez-Rodríguez, A., Stukel, M. R., Taylor, A. G. and Pasulka, A. L. (2016) Phytoplankton production and grazing balances in the Costa Rica dome. *J. Plankton Res.*, **38**, 366–379.

Landry, M. R., Selph, K. E., Stukel, M. R., Swalethorp, R., Kelly, T. B., Beatty, J. L. and Quackenbush, C. R. (this issue) Microbial food web dynamics in the oceanic Gulf of Mexico. *J. Plankton Res.*.

Landry, M. R., Selph, K. E., Taylor, A. G., Décima, M., Balch, W. M. and Bidigare, R. R. (2011) Phytoplankton growth, grazing and production balances in the HNLC equatorial Pacific. *Deep-Sea Res. II*, **58**, 524–535.

Landry, M. R., Stukel, M. R. and Décima, M. R. (2020b) Food-web fluxes support high rates of mesozooplankton respiration and production in the equatorial Pacific. *Mar. Ecol. Prog. Ser.*in press, **652**, 15–32. doi: 10.3354/meps13479.

Lindo-Atichati, D., Bringas, F., Goni, G., Muhling, B., Muller-Karger, F. E. and Habtes, S. (2012) Varying mesoscale structures influence larval fish distribution in the northern Gulf of Mexico. *Mar. Ecol. Prog. Ser.*, **463**, 245–257.

Liu, H. and Dagg, M. (2003) Interactions between nutrients, phytoplankton growth, and micro- and mesozooplankton grazing in the plume of the Mississippi River. *Mar. Ecol. Prog. Ser.*, **258**, 31–42.

Liu, H., Dagg, M. J., Wu, C.-J. and Chiang, K.-P. (2005) Mesozooplankton consumption of microplankton in the Mississippi River plume, with special emphasis on planktonic ciliates. *Mar. Ecol. Prog. Ser.*, **286**, 133–144.

Llopiz, J. K., Cowen, R. K., Hauff, M. J., Ji, R., Munday, P. L., Muhling, B. A., Peck, M. A., Richardson, D. E. *et al.* (2014) Early life history and fisheries oceanography: new questions in a changing world. *Oceanogr.*, **27**, 26–41.

López, E. and Anadón, R. (2008) Copepod communities along an Atlantic Meridional transect: abundance, size structure and grazing rates. *Deep-Sea Res. I*, **55**, 1375–1391.

Madin, L. P., Horgan, E. F. and Steinberg, D. K. (2001) Zooplankton at the Bermuda Atlantic time series study (BATS) station: diel, seasonal and interannual variation in biomass, 1994-1998. *Deep-Sea Res. II*, **48**, 2063–2082.

Melo Gonzalez, N., Muller-Karger, F. E., Cerdeira Estrada, R. S., Perez, R., Victoria, I., Cardennas Perez, P. and Arenal, I. M. (2000) Near-surface phytoplankton distribution in the western intra-Americas sea: the influence of El Nino and weather events. *J. Geophys. Res.*, **105**, 14029–14043.

Minawaga, M. and Wada, E. (1984) Stepwise enrichment of ^{15}N along food chains: further evidence and the relation between δ^{15}N and animal age. *Geochim. Cosmochim. Acta*, **48**, 1135–1140.

Merino, M. (1997) Upwelling on the Yucatan shelf: hydrographic evidence. *J. Mar. Syst.*, **13**, 101–121.

Moriarty, R. and O'Brien, T. D. (2013) Distribution of mesozooplankton biomass in the global ocean. *Earth Syst. Sci. Data*, **5**, 45–55.

Moriarty, R., Buitenhuis, E. T., Le Quére, C. and Gosselin, M.-P. (2013) Distribution of known macrozooplankton abundance and biomass in the global ocean. *Earth Syst. Sci. Data*, **5**, 241–257.

Muhling, B. A., Lamkin, J. T. and Roffer, J. T. (2010) Predicting the occurrence of Atlantic bluefin tuna (*Thunnus thynnus*) larvae in the northern Gulf of Mexico: building a classification model from archival data. *Fish. Oceanogr.*, **19**, 526–539.

Muhling, B. A., Lee, S.–. K., Lamkin, J. T. and Liu, Y. (2011) Predicting the effects of climate change on bluefin tuna (*Thunnus thynnus*) spawning habitat in the Gulf of Mexico. *ICES J. Mar. Sci.*, **68**, 1051–1062.

Owens, N. J. P. and Rees, A. P. (1989) Determination of nitrogen-15 at sub-microgram levels of nitrogen using automated continuous-flow isotope ratios mass spectrometry. *Analyst*, **114**, 1655–1657.

Roman, M. R., Adolf, H. A., Landry, M. R., Madin, L. P., Steinberg, D. K. and Zhang, X. (2002) Estimates of oceanic mesozooplankton: a comparison using the Bermuda and Hawaii time-series data. *Deep-Sea Res. II*, **49**, 175–192.

Roman, M. R., Dam, H. G., Gauzens, A. L. and Napp, J. M. (1993) Zooplankton biomass and grazing at the JGOFS Sargasso Sea time series station. *Deep-Sea Res. I*, **40**, 883–901.

Selph, K. E., Swalethorp, R., Stukel, M. R., Kelly, T. B., Knapp, A. N., Fleming, K., Hernandez, T. and Landry, M. R. (in press) Phytoplankton community composition and biomass in the open-ocean Gulf of Mexico. *J. Plankton Res.*.

Sheridan, C. C. and Landry, M. R. (2004) A 9-year increasing trend in mesozooplankton biomass at the Hawaii Ocean time-series station ALOHA. *ICES J. Mar. Sci.*, **61**, 457–463.

Shiroza, A., Malca, E., Lamkin, J. T., Gerard, T., Landry, M. R., Stukel, M. R., Laiz-Carrión, R. and Swalethorp, R. (this issue) Active prey selection in developing larvae of Atlantic Bluefin tuna (*Thunnus thynnus*) in spawning grounds of the Gulf of Mexico. *J. Plankton Res.*.

Shropshire, T., Morey, S. L., Chassignet, E., Karnauskas, M., Coles, V. J., Malca, E., Laiz-Carrión, Fiksen, O. *et al.* (this volume) Trade-offs between risks of predation and starvation in larvae make the shelf break an optimal spawning location for Atlantic Bluefin tuna. *J. Plankton Res.*.

Steinberg, D. K., Carlson, C. A., Bates, N. R., Goldthwait, S. A., Madin, L. P. and Michaels, A. F. (2000) Zooplankton vertical migration and the active transport of dissolved organic and inorganic carbon in the Sargasso Sea. *Deep-Sea Res. I*, **47**, 137–158.

Steinberg, D. K. and Landry, M. R. (2017) Zooplankton and the ocean carbon cycle. *Ann. Rev. Mar. Sci.*, **9**, 413–444.

Steinberg, D. K., Lomas, M. W. and Cope, J. S. (2012) Long-term increase in mesozooplankton biomass in the Sargasso Sea: linkage to climate and implications for food web dynamics and biogeochemical cycling. *Global Biogeochem. Cycles*, **26**, GB1004. doi: 10.1029/2010GB004026.

Straile, D. (1997) Gross growth efficiencies of protozoan and metazoan zooplankton and their dependence of food concentration, predator-prey weight ratio, and taxonomic group. *Limnol. Oceanogr.*, **42**, 1375–1385.

Strickland, J. D. H. and Parsons, T. R. (1972) *A Practical Handbook of Seawater Analysis*, Fisheries Research Board, Canada Ottawa.

Sun, D. and Wang, C. (2017) Latitudinal distribution of zooplankton communities in the western Pacific along 160°E during summer 2014. *J. Mar. Syst.*, **169**, 52–60.

Taylor, A. G., Landry, M. R., Selph, K. E. and Yang, E. J. (2011) Biomass, size structure and depth distributions of the microbial community in the eastern equatorial Pacific. *Deep-Sea Res. II*, **58**, 342–357.

Taylor, A. G., Landry, M. R., Freibott, A., Selph, K. E. and Gutiérrez-Rodríguez, A. (2016) Patterns of microbial community biomass, composition and HPLC diagnostic pigments in the Costa Rica upwelling dome. *J. Plankton Res.*, **38**, 183–198.

Valencia, B., Landry, M. R., Décima, M. and Hannides, C. C. S. (2016) Environmental drivers of mesozooplankton biomass variability in the North Pacific Subtropical Gyre. *Eur. J. Vasc. Endovasc. Surg.*, **121**, 3131–3143.

Valencia, B., Décima, M. and Landry, M. R. (2018) Environmental effects on mesozooplankton size structure and export flux at station ALOHA, North Pacific subtropical gyre. *Global Biogeochem. Cycles*, **32**, 289–305.

Yingling, N., Kelly, T. B., Selph, K. E., Landry, M. R., Knapp, A. N., Kranz, S. A. and Stukel, M. R. (this issue) Taxon-specific phytoplankton growth, nutrient limitation, and light limitation in the oligotrophic Gulf of Mexico. *J. Plankton Res.*.

Zhang, X., Dam, H. G., White, J. R. and Roman, M. R. (1995) Latitudinal variations in mesozooplankton grazing and metabolism in the central tropical Pacific during the US JGOFS EqPac study. *Deep-Sea Res. II Top. Stud. Oceanogr.*, **42**, 695–714.